Journal of Alloys and Compounds 803 (2019) 875–881

Contents lists available at ScienceDirect

Journal of Alloys and Compounds

journal homepage: http://www.elsevier.com/locate/jalcom

Electrolytic preparation and characterization of VCr alloys in molten salt from vanadium slag

Shiyuan Liu [a, b], Lijun Wang [a, c, *], Kuo-chih Chou [d], Ramachandran Vasant Kumar [c]

[a] *Collaborative Innovation Center of Steel Technology, University of Science and Technology Beijing, Beijing, 100083, China*
[b] *National Engineering Laboratory for Hydrometallurgical Cleaner Production Technology, Institute of Process Engineering, Chinese Academy of Sciences, Beijing, 100190, China*
[c] *Department of Material Science and Metallurgy, University of Cambridge, 27 Charles Babbage Road, CB3 0FS, UK*
[d] *State Key Laboratory of Advanced Metallurgy, University of Science and Technology Beijing, Beijing, 100083, China*

ARTICLE INFO

Article history:
Received 17 March 2019
Received in revised form
19 June 2019
Accepted 28 June 2019
Available online 29 June 2019

Keywords:
VCr alloy
Electrodeposition
NaCl–KCl–VCl_3–$CrCl_3$ molten salt

ABSTRACT

Vanadium slag contains several critical elements like V, Ti, Cr, Fe and Mn. In our previous work, V and Cr have been enriched by selective chlorination, increasing from 10.05% to 14.95% and 5.84%–8.69% separately. V and Cr still maintain the trivalence state in molten salt. In the current work, the electrodeposition behaviors of V^{3+} and Cr^{3+} in NaCl–KCl molten salt at 800 °C were investigated using cyclic voltammetry (CV) and square wave voltammetry (SWV) with a tungsten electrode. It was found that the reduction processes of V^{3+} and Cr^{3+} consist of two steps, M^{3+}/M^{2+}, M^{2+}/M. The diffusion coefficients of V^{3+} and Cr^{3+} in NaCl–KCl molten salt were measured by CV. The effect of $VCl_3/CrCl_3$ mass ratio on VCr alloy was investigated by a two-electrode under constant voltage. Pure Cr can be obtained at 2.8 V in the NaCl–KCl molten salt, while VCr alloy (3.71 mass % V-94.28 mass% Cr-2.01 mass % O) was obtained when electrolysis voltage was controlled to 2.8 V at 800 °C. The composition of VCr alloy can be designed by changing the molten salt composition. This method can be applied for direct preparation of VCr alloy from vanadium slag, thus offering the use of low cost raw materials with direct environmental benefits.

1. Introduction

Vanadium is a very important element. Vanadium in the form of oxides such as VO_2 can be applied to thin films and nanowire [1]. Vanadium is also important alloying element. VCr alloy is widely used as a hydrogen storage material and as a fusion reactor material [2]. In the production process of VCr alloy, the traditional method proposed is to convert V_2O_5 to the VCl_5 and reduce VCl_5 to V metallothermically by Mg. Metallic Cr is obtained from Cr_2O_3 by electrolysis or by metallothermic reduction by Si or Al. In subsequent steps, V and Cr are arc-melted over several times under an argon atmosphere and then the cast metal is pulverized. This process is highly energy-intensive and the required raw materials are high-cost pure substances [3,4]. Using ore and slag to prepare VCr alloy can reduce raw material costs. Such an approach can be considered as economically viable.

Vanadium slag generated from V-bearing titanomagnetite semlting, thus, it has been regarded as one of valuable sources due to several valuable elements inside, with an approximate composition of 13–19 mass% V_2O_3 and 1–5 mass% Cr_2O_3. Currently, in order to recover V and Cr from vanadium slag, the traditional methods convert insoluble V^{3+} or Cr^{3+} from slag to water-soluble V^{5+} or Cr^{6+} under oxidizing conditions [5–7]. The hazardous V^{5+} and Cr^{6+} may have the greatly potential to threaten the environment [8,9].

In order to effectively recover and utilize vanadium slag available in significant quantities in China, a novel process for selective extraction of iron and manganese by NH_4Cl chlorination was proposed in the present laboratory [10]. The enrichment ratio of V and Cr was obtained as 48% [11]. V and Cr elements in the enriched vanadium slag after $AlCl_3$ chlorination are presented in the form of VCl_3 and $CrCl_3$ in molten salt. VCr alloy can be obtained by molten salt electrolysis from the VCl_3 and $CrCl_3$ molten salt.

With respect to the electrochemical behavior of vanadium ions in molten salt, most of them are studied in LiCl–KCl–$TiCl_2$ system, $CaCl_2$–NaCl–VCl_2 and LiCl–KCl system [12–14]. The electrochemical behavior of Cr^{2+} and Cr^{3+} in NaCl–KCl were investigated

---

* Corresponding author. Collaborative Innovation Center of Steel Technology, University of Science and Technology Beijing, Beijing, 100083, China.
E-mail address: lijunwang@ustb.edu.cn (L. Wang).

https://doi.org/10.1016/j.jallcom.2019.06.366
0925-8388/© 2019 Published by Elsevier B.V.

[15,16]. However, the NaCl–KCl–VCl_3–$CrCl_3$ system is not reported. Meanwhile, the CV and SWV study of V and Cr in the NaCl–KCl–VCl_3–$CrCl_3$ systems are important to understand the electrochemical reactions in the salt phase and industrial electrolysis processes.

In this work, the original oxidation states of elements V and Cr are V^{3+} and Cr^{3+}. The trivalent V and Cr are reduced to alloy in one single step at relatively low temperatures. It is found that VCl_3/$CrCl_3$ mass ratios have a significant effect on the preparation of VCr alloy. In the present work, chromium-based alloys of low-oxygen content were successfully synthesized. This method can be applied for direct preparation of VCr alloy from vanadium slag, thus offering the use of low cost raw materials with direct environmental benefits.

2. Experimental section

2.1. Materials

In each experiment, the solid reagents of NaCl, KCl, VCl_3 and $CrCl_3$ used were of analytical grade. NaCl and KCl were dried at 200 °C. The Ag/AgCl electrode was used as the reference electrode (RE), which was assembled by NaCl–KCl–AgCl (2 mol%) molten salts and a half-open alumina tube (6 mm diameter). The silver wire (1 mm diameter) was inserted into the molten salt. The open end of alumina tube was sealed to prevent gas exchange. A tungsten wire (1 mm diameter) was used as the working electrode (WE). The graphite rode with the diameter of 6 mm was used as the counter electrodes (CE).

2.2. Experimental procedure

2.2.1. Electrochemical experiments

A tungsten wire (1 mm diameter) as the working electrode was held 1 cm in the molten salt. CV and SWV were carried out using a PAPSTAT 2273 electrochemical workstation and were used to explore the electrochemical properties of VCl_3 and $CrCl_3$ in the molten salt system.

2.2.2. Preparation and characterization of cathodic deposits

A near eutectic mixture of 40.4 g of NaCl and 50.4 g of KCl were mixed evenly with pre-specified weighed amounts of VCl_3 and $CrCl_3$. The alumina crucible containing the sample was placed in a shaft furnace and subjected to vacuum for 15min. The samples were heated to the 200 °C by SiC rod heating furnace and held for 24 h to drive off moisture and other volatiles, after which the samples were heated to 800 °C under a flow of high purity grade argon. In order to further purify the molten salt, a voltage lower than a decomposition voltage of molten salt is applied to electrolysis for a period of time before the electrochemical test and electrolysis. V and Cr electrolysis were carried out in the two-electrode cell at constant potential. After electrolysis, the W and graphite electrodes were pulled out from the molten salt, held 10 cm above the salt and cooled to room temperature under the protection of argon gas. The deposited product was found attaching to the surface of the W electrode. And then the products were obtained by washing with deionized water and drying. The main crystalline phase of deposited product was analyzed using X-ray diffraction (XRD) with a Cu Kα radiation source. The morphology and elemental contents of the products were observed by SEM (Zeiss Ultra 55) and EDS. The V and Cr contents of the products were analyzed by the using ICP-AES. The content of oxygen in V–Cr alloy was determined by the LECO TCH600 (The instrument LECO TCH 600 is mainly used for the measurement of medium and micro-level oxygen, hydrogen and nitrogen in steel, nonferrous metals, alloy, special metals, etc.).

3. Results and discussion

3.1. Electrolysis of V in NaCl–KCl–VCl_3 molten salt system

The dotted line in Fig. 1 is the CV of the blank NaCl–KCl molten salt at a scan rate of 200 mV/s. It can be seen from the dotted line in Fig. 1 that there is no oxidation and redox peak from 0 V to −1.8 V, and only a pair of reduction and oxidation peaks appear between −1.8 V and −2.4 V. The reduction peak and oxidation peak from the dotted line in Fig. 1 are attributed to reduction of Na^+ and oxidation of Na at the W electrode, respectively. In addition to the redox peaks of sodium, there are no other redox peaks between 0 V and −2.4 V.

In order to understand the mechanism of V^{3+} ion reduction, CV of NaCl–KCl–VCl_3 system are investigated and the results were shown in Fig. 2(a). It can be seen that two groups of signals are observed. The cathodic peaks (A and B) currents remarkably increase while the cathodic peaks (A and B) potentials clearly shift negatively with increasing scan rate.

The linear dependence of Ip on $v^{1/2}$ (v is the scan rate and Ip is the cathodic peak currents (I_A and I_B)) is shown in Fig. 2(b), suggesting that the reduction of V^{3+} ions on the W electrode are controlled by the V^{3+} ions diffusion from molten salt to the electrode surface.

Fig. 2(c) indicates variation of the cathdoic peak potential with the logarithm of the sweep rate. The cathodic peak potentials measured under increasing sweep rates shift towards a more negative value. Meanwhile, the cathodic peak potential vs. the logarithm of the sweep rate is found to be linear. The anodic peak and the cathodic peak currents corresponding to V^{3+}/V^{2+} and V^{2+}/V couples electron transfer steps can be clearly observed in Fig. 2 (a) and be regarded as quasi-reversible.

The diffusion coefficient can be calculated by the following equation when both the reactant and product are soluble [17]:

$$I_p = 0.4463 n^{\frac{3}{2}} F^{\frac{3}{2}} A (RT)^{-1/2} D^{1/2} C_0 v^{1/2} \tag{1}$$

Where F is the Faraday constant, n is the number of exchanged electrons, I_p is the peak current (A), T is the temperature in K, R is the ideal gas constant ($J\bullet mol^{-1}K^{-1}$), C_0 is the concentration of VCl_3 in the NaCl–KCl molten salt, D is the diffusion coefficient of V^{3+}, A is the surface area of W working electrode in cm^2, and v is the scan rate in V/s. The diffusion coefficient of V^{3+} is calculated as 8.72×10^{-5} cm^2s^{-1}, which is close to the values (8.22×10^{-5} cm^2s^{-1}) reported by Polovov [18].

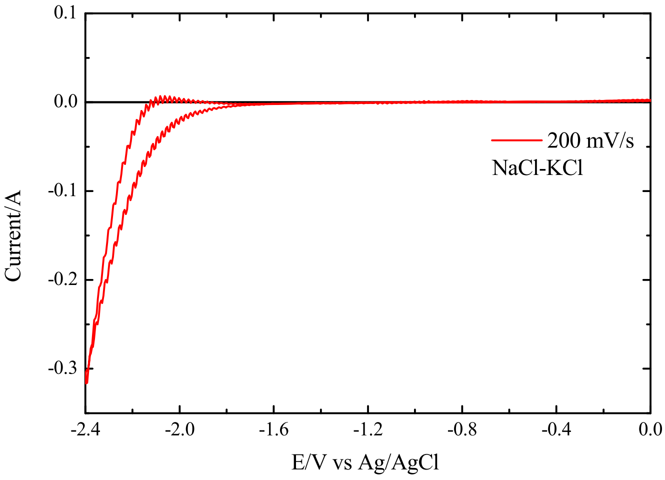

Fig. 1. The CV of blank NaCl–KCl molten salt.

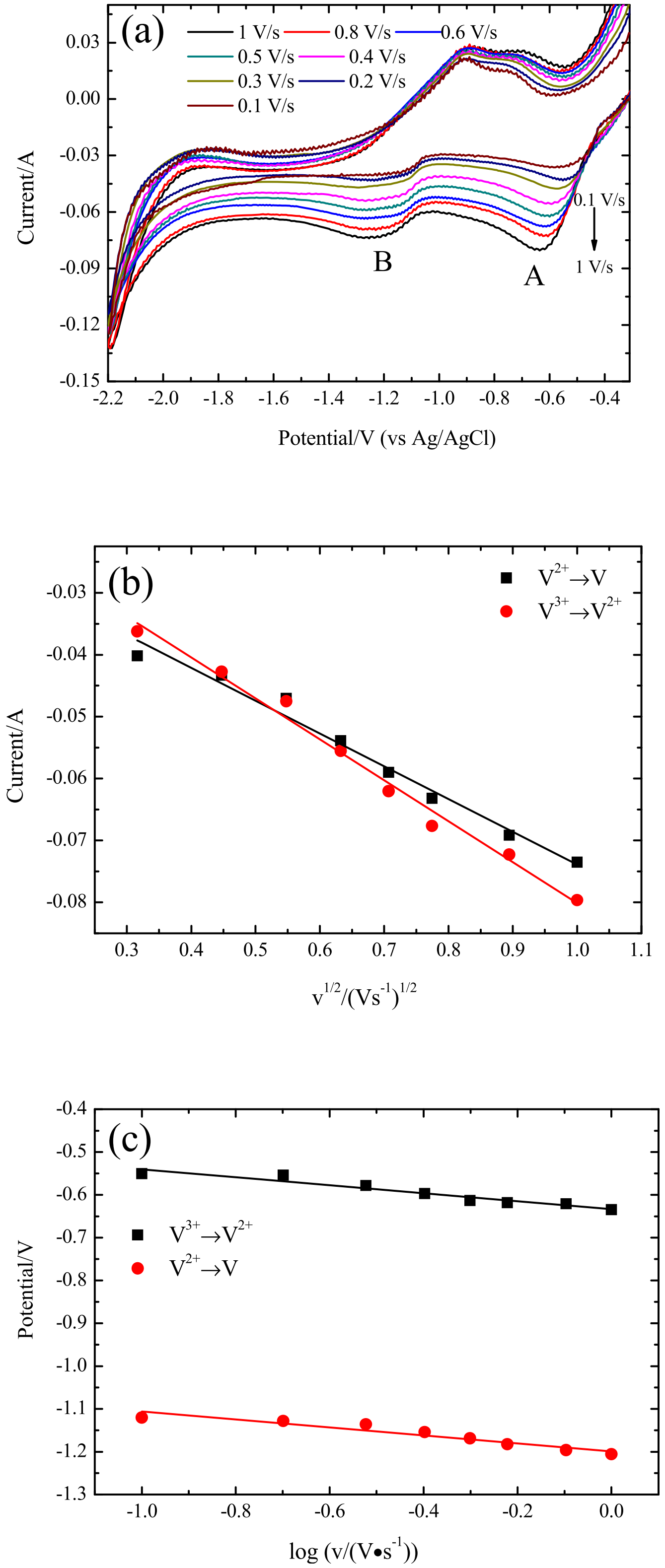

Fig. 2. (a) CV of VCl_3 (1.6 wt %) -NaCl-KCl melt on W working electrode at 800 °C; scan rate 0.1–1 $V{\bullet}s^{-1}$. (b) variation in the cathodic peak currents with the square root of the sweep rate (c) variation in cathodic peak potentials with the logarithm of the sweep rate.

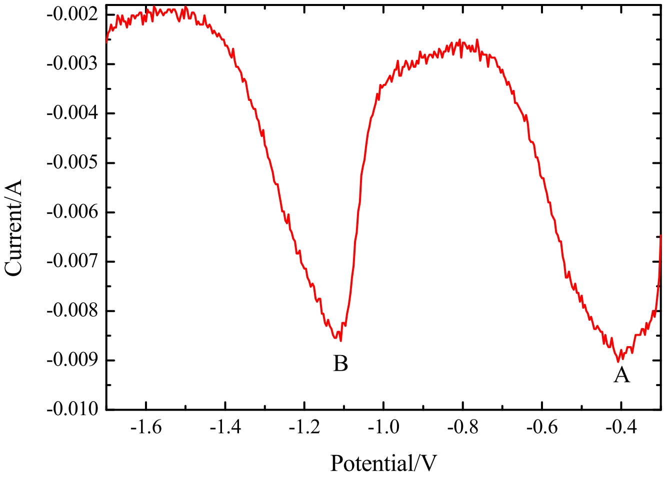

Fig. 3. SWV of NaCl–KCl–VCl_3 (1.6 wt %) melts. Working electrode: tungsten. Step potential: 3 mV. Scan rate: 200 mV/s; Temperature: 800 °C.

The diffusion coefficient could be calculated by the following equation when the product is insoluble [19]:

$$I_p = 0.61 n^{\frac{3}{2}} F^{\frac{3}{2}} A (RT)^{-1/2} D^{1/2} C_0 v^{1/2} \quad (2)$$

Where F is the Faraday constant, n is the number of exchanged electrons, I_p is the peak current (A), T is the temperature in K, R is the ideal gas constant ($J{\bullet}mol^{-1}K^{-1}$), C_0 is the concentration of VCl_2 in the NaCl–KCl molten salt, D is the diffusion coefficient of Cr^{2+}, A is the surface area of W working electrode in cm^2, and v is the scan rate in V/s. Assuming that all of the V^{3+} are converted to V^{2+}, the minimum diffusion coefficient of V^{2+} is calculated as $3.49{\times}10^{-6}$ cm^2s^{-1}.

SWV, as a sensitive transient method, was employed to investigate the electrochemical behavior of V ions in the NaCl–KCl melt. Fig. 3 shows the results obtained on the tungsten electrode at a step potential of 3 mV and scan rates of 200 mV/s in the NaCl–KCl–VCl_3 (1.6 wt%) melts at 800 °C. It can be seen from Fig. 3 that two large signals appear at −0.3987 V and −1.1222 V. The number of the corresponding exchanged electrons can be calculated according to the following equation [20]:

$$W_{1/2} = 3.52RT/nF \quad (3)$$

where $W_{1/2}$ is the width of the half peak, R is the gas constant, T is absolute temperature (K), F is the Faraday constant, and n is the number of exchanged electrons.

The computed values of n_A and n_B are 1.07 at −0.3987 V and 1.7 at −1.1222 V. Thus, it can be concluded that peaks A and B correspond to the V^{3+}/V^{2+} and V^{2+}/V couples. The two-step transfer electron number is 2.77. It can also be seen from the SWV that the V^{3+}/V^{2+} and V^{2+}/V couples electron transfer steps could be regarded as quasi-reversible at 800 °C.

3.2. Electrolysis of Cr in NaCl–KCl–$CrCl_3$ molten salt system

The CV results of NaCl–KCl–$CrCl_3$ system are shown in Fig. 4(a). When the voltage is scanned in the negative direction, three cathodic peaks (A, B and C) are observed at 800 °C. The cathodic peaks (A and B) are attributed to reduction of Cr^{3+} at the W electrode. The cathodic peaks (C) appeared in CV, which may be

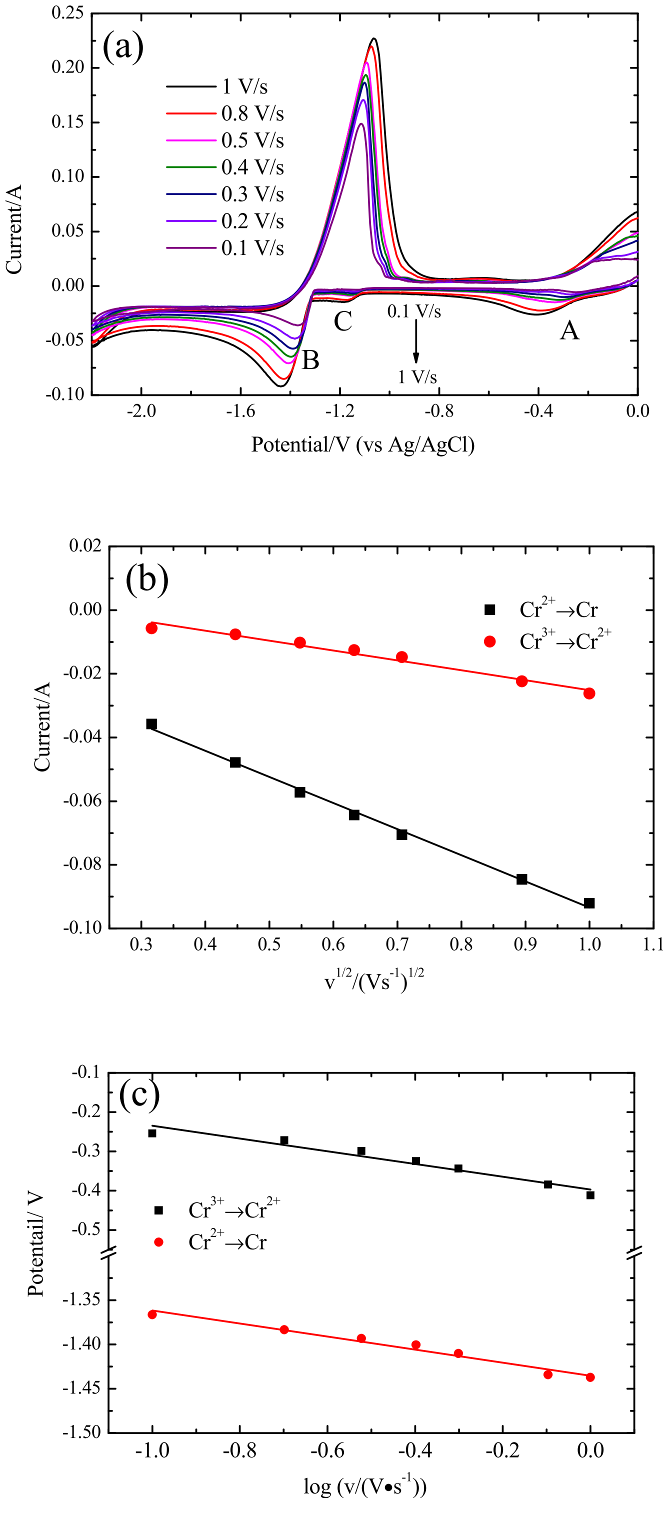

Fig. 4. (a) CV of $CrCl_3$ (1.6%)-NaCl-KCl melt on W working electrode at 800 °C; scan rate: 0.1–1 V/s (b) variation in the cathodic peak currents with the square root of the scan rate, (c) variation in cathodic peak potentials with the logarithm of the scan rate.

attributed to the formation of Cr–W alloy [21]. The cathodic peak (A and B) currents increase and the cathodic peak (A and B) potentials clearly shift negatively with the increase of the scan rate.

The linear dependence of Ip on $v^{1/2}$ (v is the scan rate and Ip is the cathodic peaks current (I_A and I_B)) is shown in Fig. 4(b). Meanwhile, Ip increases with $v^{1/2}$. This behavior from Fig. 4(b) suggests that reduction reaction of Cr ions on the W electrode are controlled by the Cr ions diffusion from molten salt to electrode surface [16,17,22].

Fig. 4(c) displays variation of the cathodic peaks potential with the logarithm of the sweep rate. The cathodic peaks potential measured under different scan rates shift towards a more negative value with increasing sweep rates. Meanwhile, the cathodic peaks potential vs. the logarithm of the sweep rate is linear. The anodic peak and cathodic peak clearly observed in Fig. 4(a) are associated with the electron transfer steps of Cr^{3+}/Cr^{2+} and Cr^{2+}/Cr couples, which can be regarded as quasi-reversible. The diffusion coefficient of Cr^{3+} is calculated as 26.5×10^{-5} cm^2s^{-1}, which is larger than the values (6.5×10^{-5} cm^2s^{-1}) reported by Ge et al. [16]. The main reason for the large data deviation is that the understanding of three peaks of chromium ions is different. Ge et al. attribute the C peak to the reduction peak of the Cr^{3+}/Cr^{2+} and the A peak to the peak of impurity oxygen ion in the molten salt. However, the source of the oxygen ion is not explained in detail. In the present work, the C-peak was interpreted as corresponding to Cr–W peak, which is in accordance with the literature [21]. Assuming that all of the Cr^{3+} in the NaCl–KCl–$CrCl_3$ are converted to Cr^{2+}, the minimum diffusion coefficient of Cr^{2+} is calculated as 8.50×10^{-6} cm^2s^{-1}.

Fig. 5 shows the SWV results obtained on the tungsten electrode at a step potential of 3 mV and scan rates of 200 mV/s in the NaCl–KCl–$CrCl_3$ (1.6 wt%) melts at 800 °C. It can be seen from Fig. 5 that three large cathodic signals have appeared at −0.3957 V, −1.239 V, and −1.348 V. Peaks A and C correspond to the Cr^{3+}/Cr^{2+} and Cr^{2+}/Cr couples. The cathodic peaks (B) appeared in CV, which may be attributed to the formation of Cr–W alloy [21].

The Fig. 6 shows the effect of electrolysis time at 2.8 V and 800 °C on current. The current declines from 3.17A to 2.04A when the voltage of 2.8 V is applied in 0.2 min, suggesting electrolytic cell has reached equilibrium. As the metal chromium deposits on the W electrode surface, the effective electrode area of W cathode increases. As the metal Cr deposits on the W electrode surface, the effective electrode area of W cathode increases. The current increases from 2.04A to 3.17 A with time up to 30 min, which can be attributed to increase in the surface area of the W cathode. The current decreases to 0.33A with time up to 105min, which was related to decline concentration of Cr^{3+}. And then, the current declines to a constant about 0.11 A with 105–166 min [23].

The XRD pattern in Fig. 7 indicates that the deposited product is pure Cr. Meanwhile, the crystal Cr oriented in (200) face has a

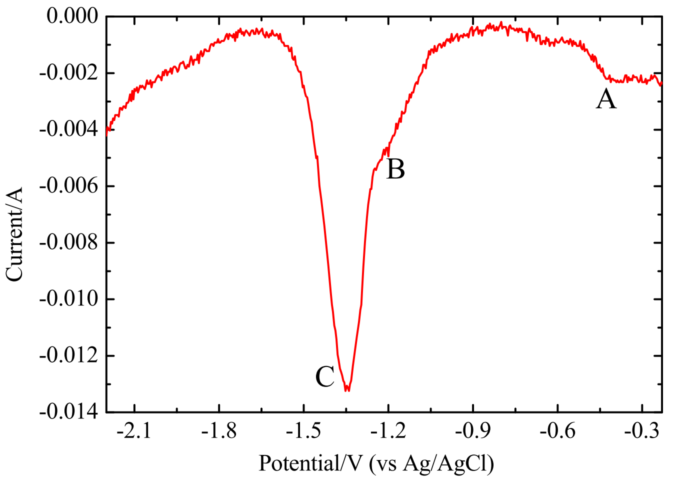

Fig. 5. SWV of NaCl–KCl–$CrCl_3$ (1.6 wt %) melts. Working electrode: tungsten. Step potential: 3 mV. Scan rate: 200 mV/s; Temperature: 800 °C.

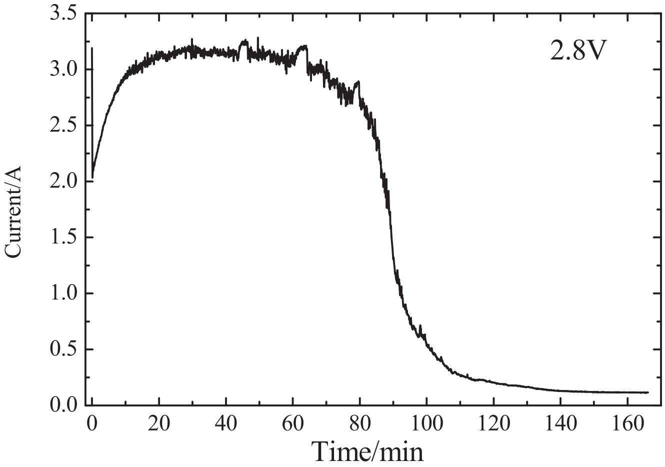

Fig. 6. Effect of time on the current in electrolysis of molten salt (NaCl–KCl–$CrCl_3$ (7.60%), 800 °C).

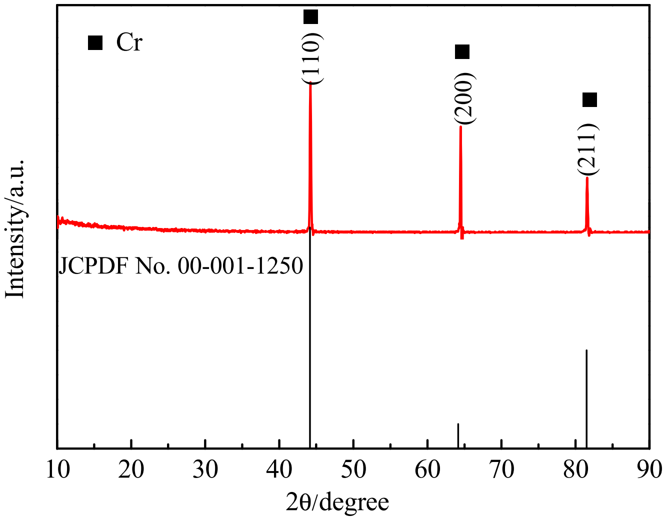

Fig. 7. XRD patterns of the deposited product (NaCl–KCl–$CrCl_3$(7.60%), 2.8 V, 800 °C).

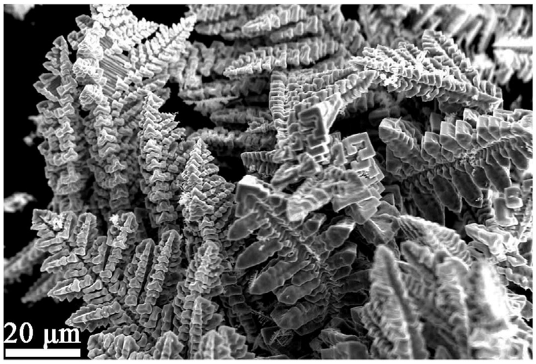

Fig. 8. SEM image of deposited product (NaCl–KCl–$CrCl_3$ (7.60%), 2.8 V, 800 °C).

preferentially growth orientation. The Fig. 8 presents the SEM morphology of the Cr product. It can be seen that the Cr formed exhibits a dendritic shape. The content of oxygen in Cr product was determined by the LECO TCH600. The mass percentages of Cr and O in the Cr product are 99.79% and 0.21% O, respectively.

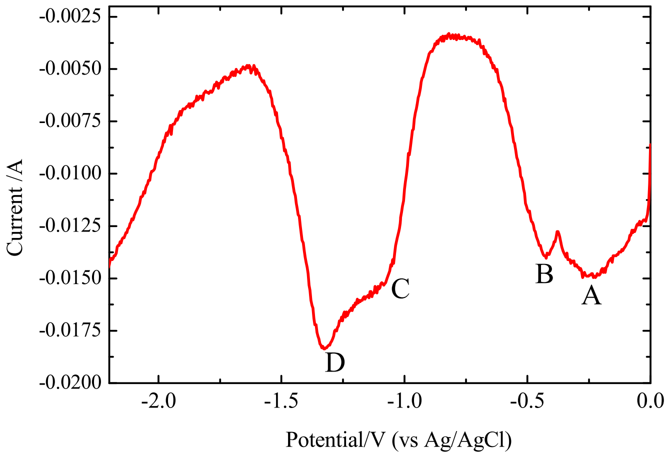

Fig. 9. SWV of NaCl–KCl–$CrCl_3$ (1.91 wt%)-VCl_3(1.91 wt %) melt. Working electrode: tungsten. Step potential: 3 mV. Scan rate: 200 mV/s; Temperature: 800 °C.

3.3. Electrochemical behaviors of $CrCl_3$ and VCl_3 in the NaCl–KCl molten salt

SWV was employed to investigate the electrochemical behaviors of V^{3+} and Cr^{3+} in the NaCl–KCl–$CrCl_3$ (1.91 wt%)-VCl_3 (1.91 wt %) melts at 800 °C and the results are in Fig. 9 obtained on the tungsten electrode at a step potential of 3 mV and scan rates of 200 mV/s. It can be seen from Fig. 9 that four large cathodic signals have appeared at −0.239 V, −0.418 V, −1.084 V, and −1.323 V, and from Fig. 3 that the cathodic peak potential of V^{3+}/V^{2+} and V^{2+}/V are −0.3987 V and −1.122 V, while the cathodic peak potential of Cr^{3+}/Cr^{2+} and Cr^{2+}/Cr were −0.3957 V and −1.348 V (Fig. 5). Thus, both Cr and V reduction takes place via two steps, and the peaks A, B, C and D correspond to Cr^{3+}/Cr^{2+}, V^{3+}/V^{2+}, V^{2+}/V and Cr^{2+}/Cr redox couples. It can be seen from Fig. 5 that Cr^{3+} is first reduced to Cr^{2+}. The peak position of Cr^{3+}/Cr^{2+} is shifted in the positive direction, arising from the presence of V^{3+}. The second reduction peak is associated with V^{3+} reduction to V^{2+}. Due to the presence of Cr^{2+} and Cr^{3+}, the peak position of V^{3+}/V^{2+} is negatively shifted. The third reduction peak is the peak of V^{2+} reduction to metallic V. The peak position of V^{2+}/V is positively shifted, which is attributed to the presence of Cr^{2+} and Cr^{3+}. The fourth peak is the peak of Cr^{2+} reduction to Cr. Due to the presence of V^{2+} and V^{3+}, the peak position of Cr^{2+}/Cr^{+} is positively shifted. The potential positive shift is due to an increasing of activity of the formed metal ions [24]. It can be also clearly seen from Fig. 9 that the peak potentials of V^{3+} and Cr^{3+} are different.

The reduction of V^{3+} and Cr^{3+} can be depicted as follows:

$$V^{3+}+3e = V \tag{4}$$

$$Cr^{3+}+3e = Cr \tag{5}$$

According to the Nernst equation [25]:

$$E_{V^{3+}/V}=E^{\theta}_{V^{3+}/V}+\frac{RT}{nF}ln\frac{a_{V^{3+}}}{a_V} \tag{6}$$

Where $a_{V^{3+}}$ and a_V are activity of V^{3+} and metal V, respectively. The activity of metal vanadium is assumed to be 1. Peak potential of V^{3+} can be shifted to more negative values from decreasing concentration of V^{3+}. Thus, co-deposition of V^{3+} and Cr^{3+} can be achieved by adjusting the concentration of V^{3+} and Cr^{3+} in the molten salt.

Based on the CV and SWV results, the co-deposition of V^{3+} and

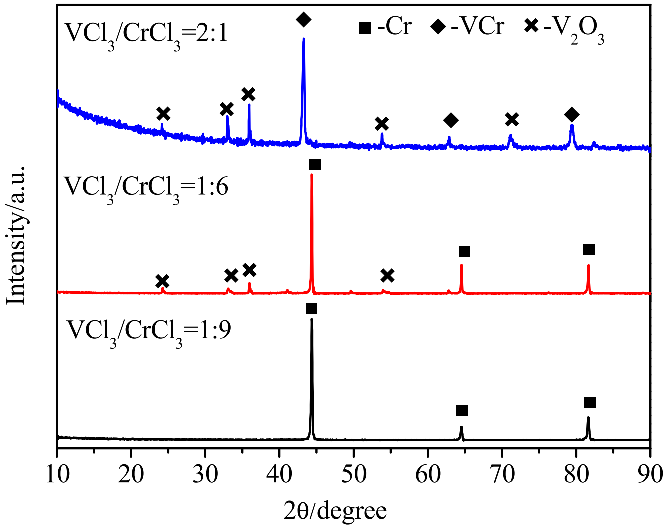

Fig. 10. XRD patterns of the deposited product at different $VCl_3/CrCl_3$ mass ratio and 800 °C for 130 min.

Cr^{3+} were performed in NaCl–KCl–VCl_3–$CrCl_3$ molten salt using a two-electrode cell at different $VCl_3/CrCl_3$ mass ratio at 800 °C. Changes in the standard Gibbs free energy formation of VCl_3 and $CrCl_3$ as a function of temperatures were calculated by the FactSage 6.4 program. According to Nernst equations, the theoretical decomposition voltage of VCl_3 and $CrCl_3$ at 800 °C are 1.18 V and 1.06 V, respectively. A higher cell voltage than the theoretical decomposition voltage is necessary for electrolysis of VCl_3 and $CrCl_3$, in order to overcome polarization at the electrodes with Cr formation at a very slightly lower voltage.

The influence of $VCl_3/CrCl_3$ mass ratio on the formation of V–Cr alloy was investigated. The electrolysis of molten salt (NaCl–KCl–$CrCl_3$–VCl_3) was performed at 800 °C for an applied potential of 2.8 V. The XRD pattern in Fig. 10 indicates that the deposited product at $VCl_3/CrCl_3$ mass ratio of 2:1 consists of a phase mixture of VCr alloy and V_2O_3. The deposited product at $VCl_3/CrCl_3$ mass ratio of 1:6 is made up of nearly pure Cr and V_2O_3, while at a mass ratio of 1:9, nearly pure Cr single phase is formed. The Fig. 11 (a)-(c) presents the SEM morphology of the deposited product at different $VCl_3/CrCl_3$ mass ratios. The EDS analyses of deposited cathode products are shown at Table 1. It can be seen that the VCr alloy and V_2O_3 at $VCl_3/CrCl_3$ mass ratio of 2:1 exhibits a granular shape. Based on the XRD analysis, the particle 1 in Fig. 11(a) is V–Cr alloy and the particle 2 in Fig. 11(a) represents V_2O_3 and V. The deposited product at $VCl_3/CrCl_3$ mass ratio of 1:6 and 1:9 in Fig. 11(b)-(c) show two different morphological crystals, viz, a granular shape and a floc. Compared with the oxygen content in the granular shape, the oxygen content in the floc increases. Although the deposited products have two different morphologies, the two forms of products are both seen to be metallic chromium. In view of the inaccuracy of the oxygen content in the sample by EDS, the content of oxygen in Cr product at $VCl_3/CrCl_3$ mass ratio of 1:9 was determined by the LECO TCH600. The mass percentages of V, Cr and O in the Cr product are 3.71%, 94.28% and 2.01% O, respectively.

Cr/V mass ratio in the VCr alloy are listed in Table 1. Fig. 12 shows the effect of varying $CrCl_3/VCl_3$ mass ratio on the resulting Cr/V mass ratio values in the VCr alloy under the operating conditions of 800 °C for 130 min. Cr/V mass ratio in the VCr alloy increased with increasing $CrCl_3/VCl_3$ mass ratio. According to Fig. 12, different ratios of V/Cr alloy can be obtained by controlling the $CrCl_3/VCl_3$ mass ratio.

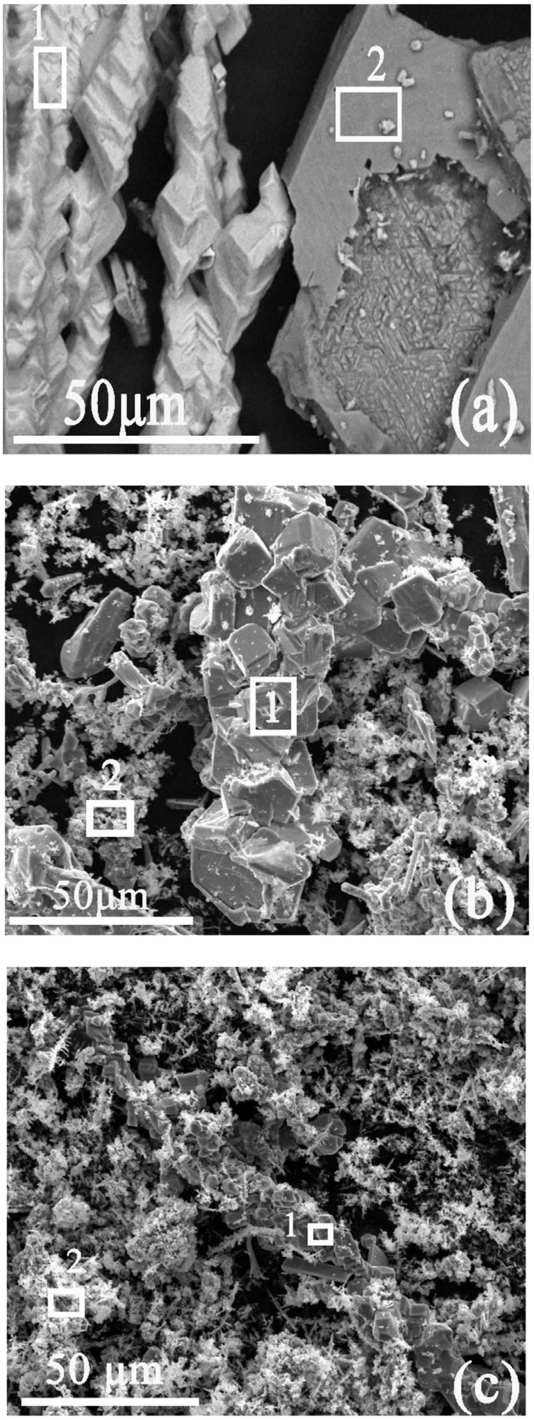

Fig. 11. SEM image of deposited product at 800 °C for 130 min (a) $VCl_3/CrCl_3$ mass ratio of 2:1, (b) $VCl_3/CrCl_3$ mass ratio of 1:6, (c) $VCl_3/CrCl_3$ mass ratio of 1:9.

In the present work, V_2O_3 detected in the deposited products is mainly attributed to oxidation of metal vanadium obtained by electrolysis. Similar results are reported in the literature [3,26].

4. Conclusions

The electrodeposition behaviors of V^{3+} and Cr^{3+} in NaCl–KCl molten salt at 800 °C were investigated using CV and SWV with a tungsten electrode. The reduction of V^{3+} ions to metal V was found

Table 1
EDS analysis of deposited product (in Fig. 11).

phase	EDS analysis of the deposited product [wt%]		
	V	Cr	O
a-1	50.79	45.43	3.78
a-2	88.61	0	11.39
b-1	3.93	95.10	0.97
b-2	8.66	85.24	6.10
c-1	3.68	93.42	2.90
c-2	4.79	90.08	5.13

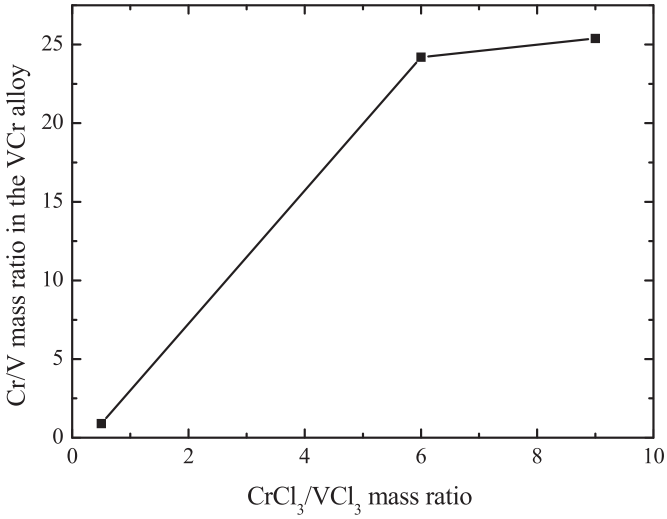

Fig. 12. Effect of different $CrCl_3/VCl_3$ mass ratio on Cr/V mass ratio in the VCr alloy at 800 °C for 130 min.

to take place in two steps corresponding to V^{3+}/V^{2+} and V^{2+}/V. The reduction of Cr^{3+} ions to metal Cr similar involved redox steps of Cr^{3+}/Cr^{2+} and Cr^{2+}/Cr. The electrochemical processes of V^{3+} and Cr^{3+} were proved to be controlled by diffusion. The diffusion coefficients of V^{3+} and Cr^{3+} in NaCl−KCl molten salt were 8.72×10^{-5} cm^2s^{-1} and 26.5×10^{-5} cm^2s^{-1}. Based on the CV and SWV analysis, electrodeposition of Cr was investigated by a two-electrode arrangement under constant voltage, and pure Cr was obtained. Meanwhile, the effect of $VCl_3/CrCl_3$ mass ratio on VCr alloy was investigated by a two-electrode cell under constant voltage. It was found that $VCl_3/CrCl_3$ mass ratio significantly affected the purity of product. V_2O_3 detected in the deposited products is mainly attributed to oxidation of metal vanadium obtained by electrolysis. VCr alloy (3.71 mass % V, 94.28 mass% Cr and 2.01 mass % O) was obtained when electrolysis voltage was controlled at 2.8 V at 800 °C.

Acknowledgments

The authors are grateful for the financial support of this work from the National Natural Science Foundation of China (No.51474141, 51774027), and China Postdoctoral Science Foundation (2019M650848).

References

[1] K. Liu, S. Lee, S. Yang, O. Delaire, J.Q. Wu, Recent progresses on physics and applications of vanadium dioxide, Mater. Today 21 (8) (2018) 875−896.

[2] K. Edalati, M. Novelli, S. Itano, H.W. Li, E. Akiba, Z.J. Horita, T. Grosdidier, Effect of gradient-structure versus uniform nanostructure on hydrogen storage of Ti-V-Cr alloys: investigation using ultrasonic SMAT and HPT process, J. Alloy. Comp. 737 (2018) 337−346.

[3] R.O. Suzuki, K. Tatemote, H. Kitagawa, Direct synthesis of the hydrogen storage V-Ti alloy powder from the oxides by calcium co-reduction, J. Alloy. Comp. 385 (2004) 173−180.

[4] V.N. Verbetsky, T.A. Zotov, A.V. Tatarintsev, E.A. Movlaev, Hydrogen sorption properties of $V_{1-x}Cr_x$ (x=0.1−0.5) alloys, Inorg. Mater. 49 (2) (2013) 149−152.

[5] Y.L. Ji, S.B. Shen, J.H. Liu, S.Y. Yan, Z.T. Zhang, Green and efficient process for extracting chromium from vanadium slag by an innovative three-phase roasting reaction, ACS Sustain. Chem. Eng. 5 (7) (2017) 6008−6015.

[6] J.Y. Xiang, Q.Y. Huang, X.W. Lv, C.G. Bai, Extraction of vanadium from converter slag by two-step sulfuric acid leaching process, J. Clean. Prod. 170 (2018) 1089−1101.

[7] T. Jiang, J. Wen, M. Zhou, X.X. Xue, Phase evolutions, microstructure and reaction mechanism during calcification roasting of high chromium vanadium slag, J. Alloy. Comp. 742 (2018) 402−412.

[8] M. Sturini, E. Rivagli, F. Maraschi, A. Speltini, A. Profumo, A. Albini, Photocatalytic reduction of vanadium (V) in TiO_2 suspension: chemometric optimization and application to wastewaters, J. Hazard Mater. 254−255 (2013) 179−184.

[9] Z.H. Diao, X.R. Xu, H. Chen, D. Jiang, Y.X. Yang, L.J. Kong, Y.X. Sun, Y.X. Hu, Q.W. Hao, L. Liu, Simultaneous removal of Cr(VI) and phenol by persulfate activated with bentonite-supported nanoscale zero-valent iron: reactivity and mechanism, J. Hazard Mater. 316 (2016) 186−193.

[10] S.Y. Liu, S.J. Li, S. Wu, L.J. Wang, K.C. Chou, A novel method for vanadium slag comprehensive utilization to synthesize Zn-Mn ferrite and Fe-V-Cr alloy, J. Hazard Mater. 354 (2018) 99−106.

[11] S.Y. Liu, L.J. Wang, K.C. Chou, Selective chlorinated extraction of iron and manganese from vanadium slag and their application to hydrothermal synthesis of $MnFe_2O_4$, ACS Sustain. Chem. Eng. 5 (2017) 10588−10596.

[12] K. Milicevic, B. Friedrich, J. Gussone, J. Haubrich, Anodic dissolution of vanadium in molten LiCl-KCl-$TiCl_2$, J. Appl. Electrochem. 47 (2017) 573−581.

[13] P.K. Tripathy, Electrochemical refining of carbonitrothermic vanadium in $CaCl_2$-NaCl-VCl_2 electrolytic bath, Miner. Process. Extr. Metall. (Trans. Inst. Min. Metall. C). 120 (2) (2011) 90−96.

[14] J. Gussone, C.R.Y. Vijay, J. Haubrich, K. Milicevic, B. Friedrich, Effect of vanadium ion valence state on the deposition behavior in molten salt electrolysis, J. Appl. Electrochem. 48 (2018) 427−434.

[15] W. Liu, G.L. Liu, S.J. Xiao, J. Zhang, The electrochemical behavior of Cr(II) ions in NaCl-KCl melt, Int. J. Electrochem. Sci. 12 (2017) 1589−1599.

[16] X.L. Ge, S.J. Xiao, G.M. Haarberg, S. Seetharaman, Salt extraction process−novel route for metal extraction Part 3−electrochemical behaviours of metal ions (Cr, Cu, Fe, Mg, Mn) in molten ($CaCl_2$−)NaCl−KCl salt system, Trans. Inst. Min. Metall. C. 119 (3) (2010) 163−170.

[17] Q.C. Yan, X.M. Guo, Preparation and characterization of Sm_2Fe_{17} alloy in LiF-CaF_2-SmF_3 molten salt, J. Alloy. Comp. 747 (2018) 994−1001.

[18] I.B. Polovov, M.E. Tray, M.V. Chernyshov, V.A. Volkovich, B.D. Vasin, O.I. Rebrin, Electrode Processes in Vanadium-Containing Chloride Melts. Molten Salts Chemistry and Technology, Wiley, Hoboken, 2014, pp. 257−281.

[19] D. Quaranta, L. Massot, M. Gibilaro, E. Mendes, J. Serp, P. Chamelot, Zirconium(IV) electrochemical behavior in molten LiF-NaF, Electrochim. Acta 265 (2018) 586−593.

[20] L. Wang, Y.L. Liu, K. Liu, S.L. Tang, L.Y. Yuan, L.L. Su, Z.F. Chai, W.Q. Shi, Electrochemical extraction of cerium from CeO_2 assisted by $AlCl_3$ in molten LiCl-KCl, Electrochim. Acta 147 (2014) 385−391.

[21] W. Liu, S.J. Xiao, Z. Wang, Electrochemical behavior of Cr(II) ion in NaCl-KCl melt at W electrode, Chin. J. Process Eng. 17 (1) (2017) 119−122 (In Chinese).

[22] A. Cotarta, Electrochemistry of molten LiCl-KCl-$CrCl_3$ and LiCl-KCl-$CrCl_2$ mixtures, J. Appl. Electrochem. 27 (1997) 651−658.

[23] X.L. Zou, X.G. Lu, C.H. Li, Z.F. Zhou, A direct electrochemical route from oxides to Ti-Si intermetallics, Electrochim. Acta 55 (2010) 5173−5179.

[24] K. Ye, M.L. Zhang, Y. Chen, W. Han, Y.D. Yan, S.Q. Wei, L.J. Chen, Study on the preparation of Mg−Li−Mn alloys by electrochemical codeposition from LiCl−KCl−$MgCl_2$−$MnCl_2$ molten salt, J. Appl. Electrochem. 40 (2010) 1387−1393.

[25] M. Li, Q.Q. Gu, W. Han, Y.D. Yan, M.L. Zhang, Y. Sun, W.Q. Shi, Electrodeposition of Tb on Mo and Al electrodes: thermodynamic properties of $TbCl_3$ and $TbAl_2$ in the LiCl-KCl eutectic melts, Electrochim. Acta 167 (2015) 139−146.

[26] L.Y. Liu, Y.D. Yan, W. Han, M.L. Zhang, L.Y. Yuan, R.S. Lin, G.A. Ye, H. He, Z.F. Chai, W.Q. Shi, Electrochemical separation of Th from ThO_2 and Eu_2O_3 assisted by $AlCl_3$ in molten LiCl−KCl, Electrochim. Acta 114 (2013) 180−188.